Metabolic Imaging by Hyperpolarized ^{13}C Magnetic Resonance Imaging for *In vivo* Tumor Diagnosis

Klaes Golman, René in't Zandt, Mathilde Lerche, Rikard Pehrson, and Jan Henrik Ardenkjaer-Larsen

Amersham Health R&D AB (Part of GE Healthcare), Malmö, Sweden

Abstract

The "Warburg effect," an elevation in aerobic glycolysis, may be a fundamental property of cancer cells. For cancer diagnosis and treatment, it would be valuable if elevated glycolytic metabolism could be quantified in an image in animals and humans. The pyruvate molecule is at the metabolic crossroad for energy delivery inside the cell, and with a noninvasive measurement of the relative transformation of pyruvate into lactate and alanine within a biologically relevant time frame (seconds), it may be possible to quantify the glycolytic status of the cells. We have examined the metabolism after i.v. injection of hyperpolarized ^{13}C-pyruvate in rats with implanted P22 tumors. The strongly enhanced nuclear magnetic resonance signal generated by the hyperpolarization techniques allows mapping of pyruvate, lactate, and alanine in a $5 \times 5 \times 10$ mm^3 imaging voxel using a 1.5 T magnetic resonance scanner. The magnetic resonance scanning (chemical shift imaging) was initiated 24 seconds after the pyruvate injection and had a duration of 14 seconds. All implanted tumors showed significantly higher lactate content than the normal tissue. The results indicate that noninvasive quantification of localized Warburg effect may be possible. (Cancer Res 2006; 66(22): 10855-60)

Introduction

Tumors have many varied characteristics. They can arise from a variety of sites within the body and develop differently. Consequently, no single test or method can accurately diagnose tumors. A series of diagnostic methods are necessary to determine whether a person has cancer.

Tumors are localized and diagnosed based on general characteristics of the malignant tissue, using all modern imaging modalities, such as X-ray, ultrasound, single-photon emission computed tomography, positron emission tomography (PET), magnetic resonance imaging (MRI), and computed tomography (CT) with or without use of contrast media injections. Because tumor tissue has a distinct morphology compared with non-tumor parental tissue (normal tissue), these morphologic changes have been the basis of tumor diagnosis using X-ray, ultrasound, CT, and MRI (1). During recent years, knowledge of contrast media pharmacokinetics have greatly improved identification and interpretation of tumor tissue using CT and MRI techniques (2). This is because the pharmacokinetics of the contrast medium correlates with perfusion, microvascular architecture, and cell membrane characteristics. Cancer tissue shows a high signal in contrast-enhanced CT and MRI corresponding to a higher concentration of contrast medium. This is especially so in cancer tissue of high malignancy as this tissue has highly permeable blood vessels and is edematous (3).

In addition to the fundamental morphologic changes, another common characteristic of cancer tissue is a high rate of aerobic glycolysis (4). Although this so-called Warburg effect (5) or hyperglycolytic state is not seen in all cancers, it seems to be a common phenotype in rapidly growing tumors (4, 6). Energy production in some cancer cells has been found to be >400-fold higher than the energy demands of the biosynthesis (7).

^{18}FDG-PET has recently gained wide acceptance for its ability to diagnose cancer. The chemical structure of ^{18}FDG is so similar to glucose that it is transported into hyperglycolytic tumor cells by the same mechanism. The fluorinated analogue of 3-deoxyglucose is taken up by the cells and metabolized into 3-deoxyglucose-6-phosphate, which is trapped inside the cell. The "hotspots" in the ^{18}FDG-PET image indicate areas of high glucose transport. PET, therefore, may indirectly report on glycolytic activity.

Magnetic resonance spectroscopy (MRS) complements PET in the diagnosis of tumor tissue based on metabolic activity. With MRS, it is possible to image and quantify certain metabolites. Cancer cells exhibit major changes in intermediary metabolism (8), and MRS, which may describe intermediary metabolism both qualitatively and quantitatively, has been used for tumor diagnosis (9). The use of MRS to diagnose especially human brain cancer has proved to be very efficient because the metabolic profiles of different tumor types are different from normal cells (10). The combination of MRS with dynamic Gd contrast-enhanced MRI yields an even more powerful diagnostic tool (11). Obstacles to extended use of MRS and MRI for tumor diagnosis in a routine clinical setting have been the inherently low nuclear magnetic resonance (NMR) signal recorded with these techniques, the complexity of the technique, and the lack of well-characterized markers that can diagnose the individual patient noninvasively.

Recently, a combination of MRS, MRI, and a hyperpolarization method [dynamic nuclear polarization (DNP)] has been reported that promises to enhance the available signal for these methods (12). The significant improvement of the signal strength for some MR-detectable compounds allows for metabolic imaging on a very short time scale. Provided the compound can be hyperpolarized by the DNP hyperpolarization technique (13), and it meets required biological criteria, it may be possible to significantly extend the use of metabolic imaging within tumor diagnosis.

The DNP hyperpolarization technique allows signal enhancement of many ^{13}C-labeled substances. Because the hyperglycolic state may be a fundamental property of cancer cells, we have chosen to study a substrate important for energy production: pyruvate. We want in this article to examine the possibility to map

Requests for reprints: Jan Ardenkjaer-Larsen, GE Healthcare, The Grove Centre (GC/18), White Lion Road, Amersham, Buckinghamshire HP7 9LL, England. Phone: 792-0210-211; E-mail: jan.henrik.ardenkjaer-larsen@ge.com.

doi:10.1158/0008-5472.CAN-06-2564

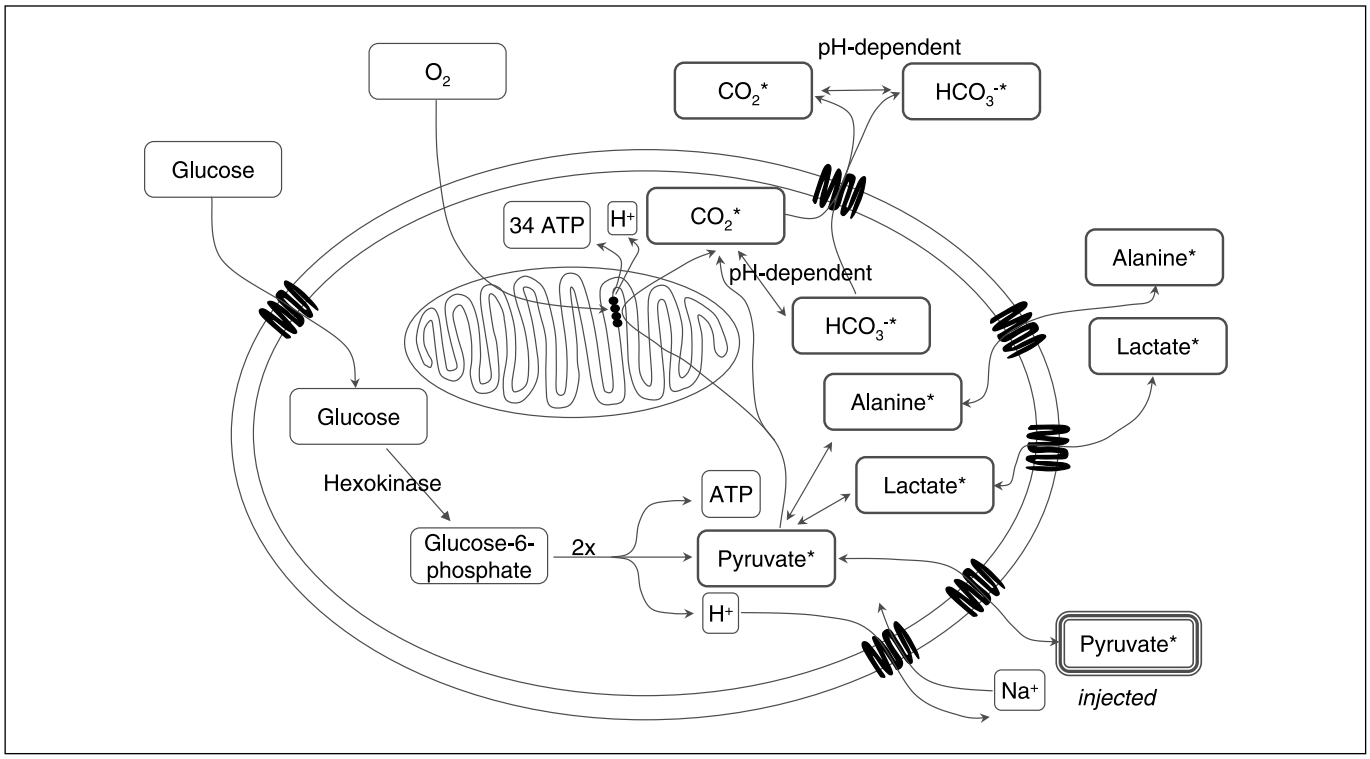

Figure 1. Overview of the major energetic metabolic pathway of the cell. Injection of $^{13}C_1$-pyruvate will result in the production of $^{13}C_1$-Lactate, $^{13}C_1$-alanine, $^{13}CO_2$, and $H^{13}CO_3^-$. Production of ATP relies strongly on the oxidative metabolism in the mitochondrion. Any disturbance in the oxidative phosphorylation requires an up-regulation of the anaerobic energy production. The hypothesis is that this can be studied by injecting $^{13}C_1$-pyruvate and observing its metabolic products.

the metabolic fate of pyruvate in an image of tumor-bearing animals using the DNP-MR technique.

Because pyruvate is at a crossroad of the major energy-generating metabolic pathways in mammalian cells (Fig. 1), the metabolism of pyruvate is expected to differ in cancer and normal cells. It is known that in cancer cells, pyruvate is abundantly transformed to lactate through anaerobic glycolysis (14). In previous studies of normal tissue (15), it is reported that both lactate and alanine are produced from injected hyperpolarized pyruvate. This makes it possible to acquire images of lactate and alanine formed from the pyruvate present in the cells and thereby map the metabolic pattern of these three metabolites.

It is the aim of the present study to determine whether it is possible to identify and characterize tumor tissue by injection of ^{13}C-labeled pyruvate and a subsequent mapping of its main metabolites.

Materials and Methods

Tumor preparation. A total of six male BDIX rats (Harlan Scandinavia, Allerød, Denmark) weighing 250 to 350 g were used. A frozen tissue suspension of a P22 tumor in RPMI 1640, 10% FCS, and 10% DMSO was brought to 37°C, and 0.5 mL was injected s.c. on the back of the rats. After 19 days, the rats were anesthetized and decapitated, and the tumors were immersed in 0.9% NaCl. Under a stereomicroscope, viable neoplastic tissue was cut into ~2-mm pieces. These pieces were engrafted into the abdomen of 10 rats by means of a silk ligature (Fig. 2). The rats were imaged 11 to 14 days later. All animal experiments were approved by the local ethical committee.

MR experiments. The rats were anesthetized using isoflurane (2-3% in oxygen) and kept on a heated table. Care was taken to ensure a body temperature of 37°C. A catheter was introduced into the tail vein, and another catheter was inserted into the Arteria carotis communis sinistra. They were then placed in the MR instrument on a home-built pad that was heated to 37°C by means of circulating FC-104 Fluorinert. This fluid will not give rise to background signals in proton and carbon MR experiments. Anesthesia was continued by means of isoflurane delivered via a long tube to an open-breathing system (1-2%, 0.4 L min^{-1}). The arterial catheter was

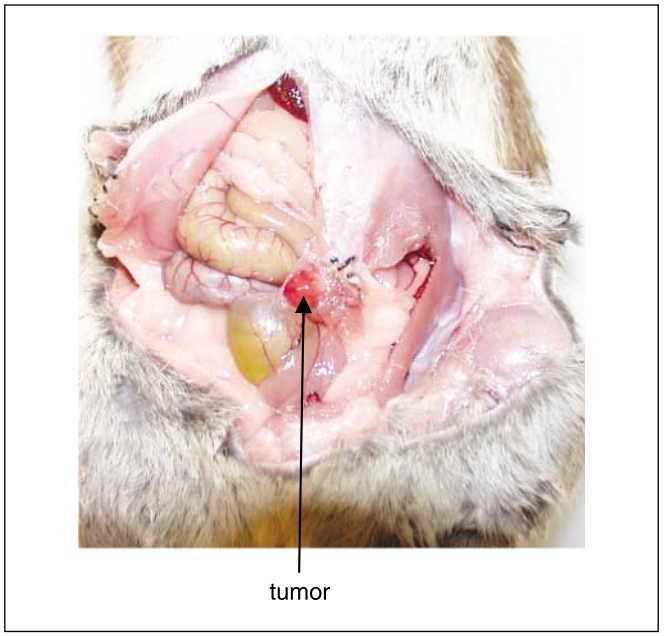

Figure 2. Photograph of the viable neoplastic tissue P22. The tissue was engrafted into the abdomen of the animal by means of a silk ligature.

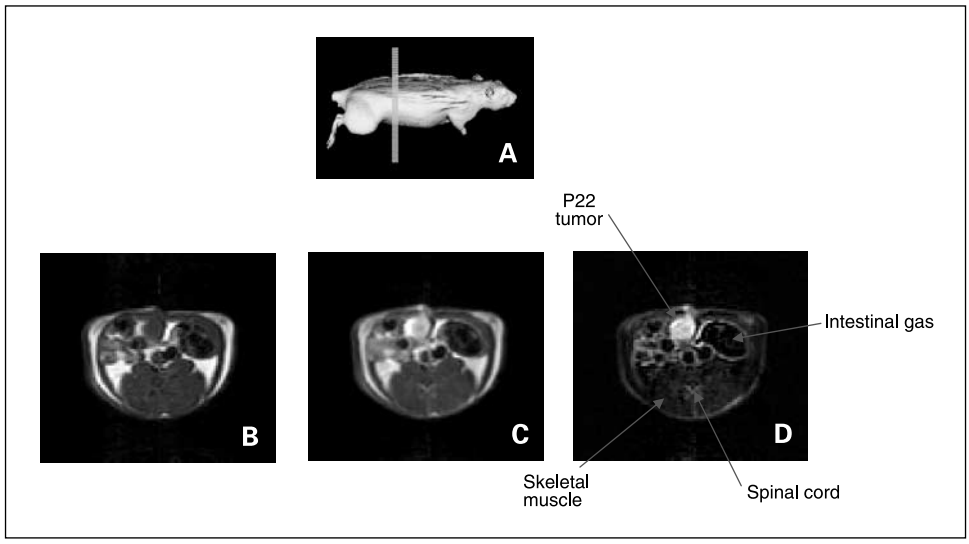

Figure 3. Enhancement of the neoplastic P22 tissue using Omniscan. *A,* the location of the image slab in the rat and the corresponding transversal ^{1}H-NMR image. *B,* pre-contrast image. *C,* post-contrast image. *D,* difference image, clearly showing the homogenous enhancement of the P22 tumor.

connected via a T-tube to a pressure recorder and a pump delivering saline (0.15 L min^{-1}) to prevent catheter clotting. The body temperature and blood pressure were continuously recorded during the experiments.

Rats were positioned in a 1.5-T clinical MRI (Siemens Sonata, Siemens, Erlangen, Germany) using a ^{1}H-^{13}C T_x/R_x birdcage coil (diameter = 8.3 cm, length = 10 cm; Rapid Biomedical GmbH, Rimpar, Germany) and imaged using a standard proton MR imaging sequence to get the anatomic information and the location of the tumor. All automatic in line adjustments of the MR scanner were disabled. This was done to avoid unwanted radiofrequency pulses, which would destroy the hyperpolarization signal. A 90-degree reference radiofrequency pulse was calibrated using the natural abundance ^{13}C-lipid signal. Based on the proton frequency found by the MR system, the MR frequency for $^{13}C_1$-alanine was calculated. This frequency will position the MR signal arising from $^{13}C_1$-alanine in the middle of the ^{13}C-MR spectrum with $^{13}C_1$-lactate on the left and $^{13}C_1$-pyruvate resonating on the right of $^{13}C_1$-alanine. A nonlocalized MR spectroscopy sequence was run for setting of the ^{13}C-MR coil and the system MR frequency. The chemical shift imaging (CSI) was based on a standard sequence (Siemens V21B) with a few modifications, including a centric K-space acquisition and a possibility to change the repetition time to short values (as short as the sequence would allow, T_R = 90 milliseconds). The ^{13}C-image location was chosen to cover the tumor (slice thickness = 10 mm, in plane pixel size = 5 × 5 mm^2). In the reconstruction phase, the image data was "zero-filled" to result in 2.5 × 2.5 × 10 mm^3 resolution.

Imaging substances. $^{13}C_1$-pyruvate was hyperpolarized in a polarizer using the technique as previously described (15), and the sample was subsequently dissolved in an aqueous solution of sodium hydroxide and TRIS buffer to provide a 79 mmol/L solution of hyperpolarized sodium $^{13}C_1$-pyruvate with a pH of 8.2 and a polarization of ~20% during the administration.

The given dose of 0.79 mmol/kg was infused during 14 seconds. Thirty seconds after start of the infusion, a CSI sequence was started. The CSI sequence (12 seconds) was done as previously described (15).

The Gd contrast medium gadodiamide (Omniscan, GE Healthcare, Little Chalfont, United Kingdom) was diluted five times with sterile water. The diluted MRI contrast medium was then injected (0.4 mmol/kg) during 2 seconds, and a standard T_1 weighed proton spin echo imaging sequence (T_E = 14 milliseconds, T_R = 500 milliseconds, field of view = 217 × 163 mm^2, slice thickness = 3 mm, 256 × 192 matrix) was used to measure the contrast changes due to the Gd contrast medium. The imaged slice was chosen to cover the same area as the ^{13}C-imaging slice, and post-contrast images were acquired 40 seconds after the start of the injection.

These contrast-enhanced proton images were used as reference morphologic images localizing the position of the tumor and securing that the tumor was well perfused.

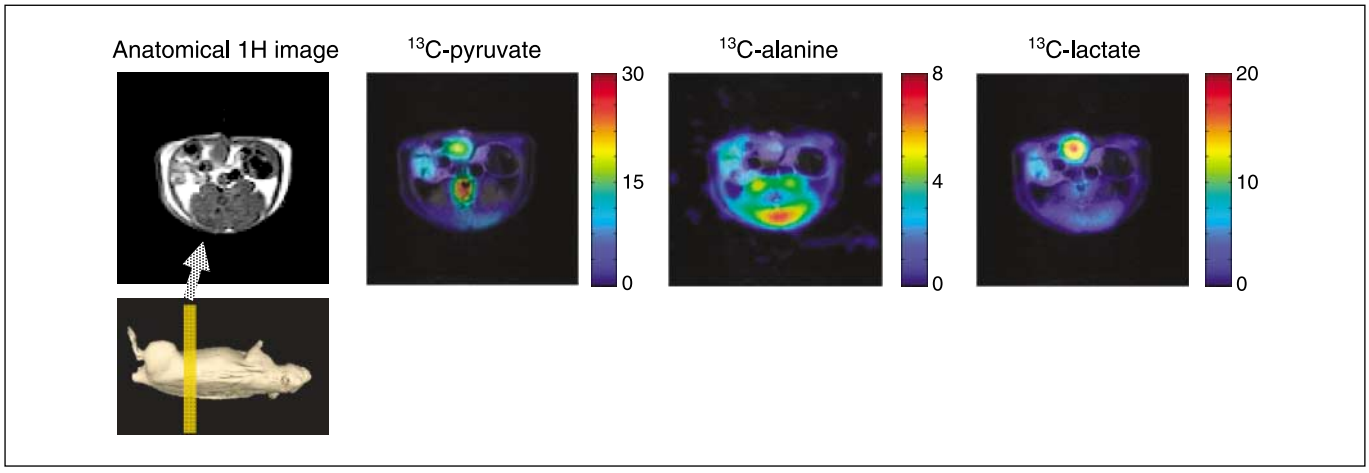

Figure 4. Location of the image slab in the rat and the corresponding transversal ^{1}H-NMR image. The NMR signal distribution obtained simultaneously from pyruvate, lactate, and alanine is calculated, and the color images representing the intensity of each metabolite are projected on the anatomical ^{1}H image. Alanine is most prominent in the skeletal muscle around the spinal cord, whereas the P22 tumor tissue is indicated by the highest signal for lactate. Note the different scale.

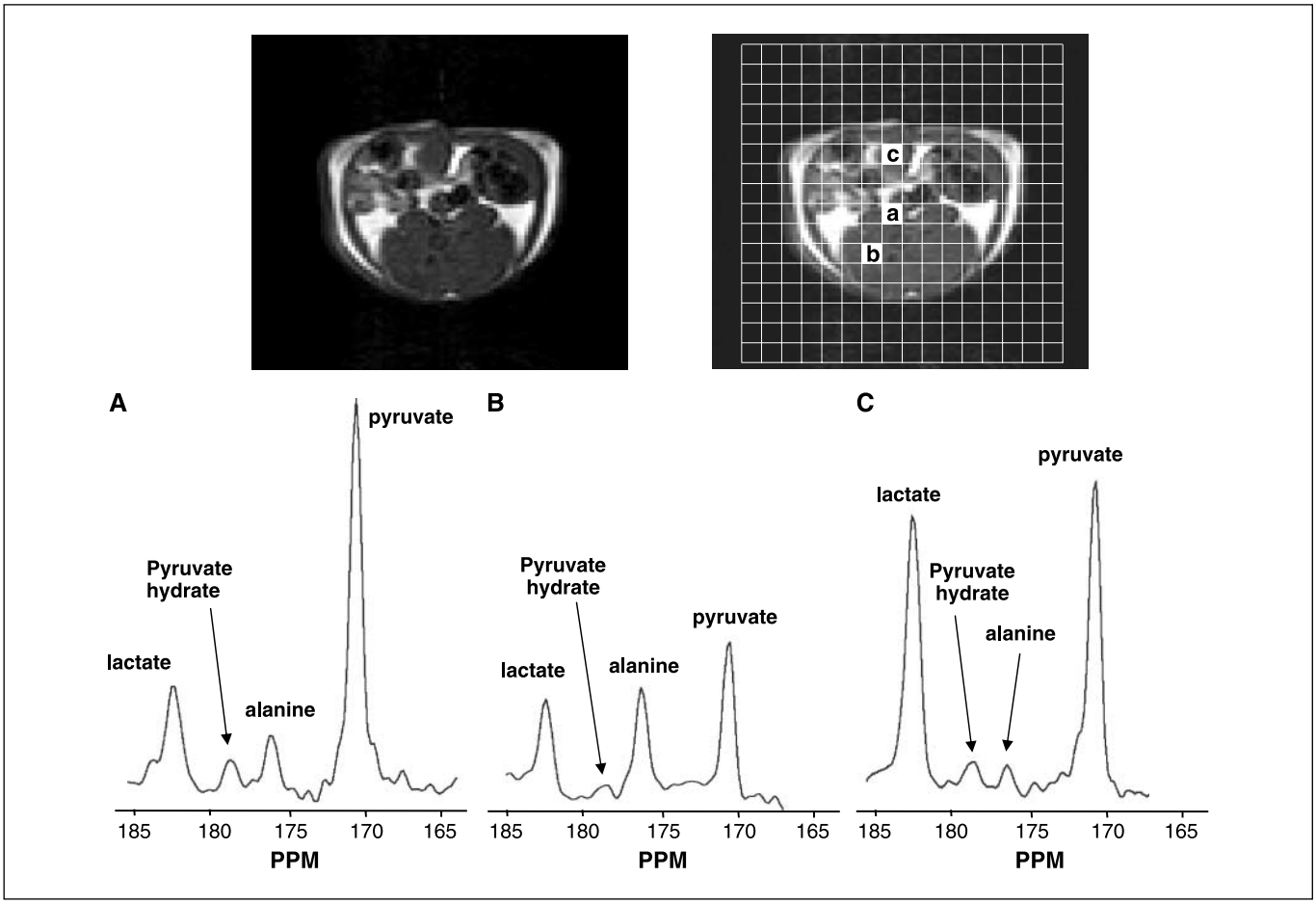

Figure 5. Change of metabolic pattern visualized by the $^{13}C_1$-MR spectra originating from the area containing vena cave (*A*), skeletal muscle (*B*), and P22 tumor tissue (*C*). Whereas alanine is most prominent in skeletal muscle, the tumor shows a typical lack of alanine signal and has a high lactate signal.

Processing imaging data. The metabolic images were calculated from the CSI data set using a home-written program coded in Matlab 6.5.1 (Mathworks Inc., Natick, MA). This program incorporates time domain fitting algorithms (16). After manual phasing of the spectra, the amplitudes were estimated assuming constant phase; identical line width for alanine, lactate, and pyruvate; and a fixed frequency shift between lactate and alanine (106 Hz) and pyruvate and alanine (−92 Hz).

Macroscopic and histologic examinations. After completion of the MR experiments, the animals were sacrificed with pentobarbital i.v., and tumors were removed for histology. Only animals having tumors with homogenous tissue composition and with tumors that were >100 mg were included in the experiments. Histology confirmed all included tumors to be neoplastic.

Results

Gadodiamide-enhanced proton images were collected from all animals. These images show a homogenous enhancement within the tumor, indicating well-perfused and homogenous tumors (Fig. 3).

The distribution of $^{13}C_1$-pyruvate and its metabolites $^{13}C_1$-alanine and $^{13}C_1$-lactate was imaged 30 to 44 seconds after the start of the administration of pyruvate (Fig. 4). A distribution of pyruvate has taken place within the time frame of ~0.5 minute (Fig. 4), and the highest signal originates from the well-perfused tumor and aorta. Pyruvate has been partly metabolized into alanine and lactate. Figure 4 shows the distribution of lactate from which it can be seen that the tumor area contains the highest concentration of lactate. Figure 4 shows that the metabolism of pyruvate into alanine is dominating in the muscle, and that alanine production is very low in the tumor. Generally, it can be seen from the images that pyruvate metabolism is dependent on organ type.

To qualitatively evaluate the relative amounts of the three metabolites in different tissue types, the spectra obtained from three different tissue types are shown in Fig. 5. The voxel depicted in Fig. 5*A* mainly contains blood but is also contaminated with other tissue types. The content of pyruvate dominates the spectrum. In Fig. 5*B*, the voxel shown covers muscle tissue and contains almost equal amounts of all three metabolites. The third voxel (Fig. 5*C*) covers the tumor and contains almost equal amounts of lactate and pyruvate and insignificant amounts of alanine. From Fig. 4, it can also be seen that not only do the absolute amounts of the metabolites differ, but the relative amounts of the metabolites also vary significantly between tissue types. The difference in metabolic profile between skeletal muscle and tumor tissue is visualized in Fig. 6 in which the amplitudes for the metabolites lactate, alanine, and pyruvate are plotted against each other for each of the 10 animals. The distribution of the metabolites shows a segregated relation between the metabolic concentrations for skeletal muscle and tumor tissue.

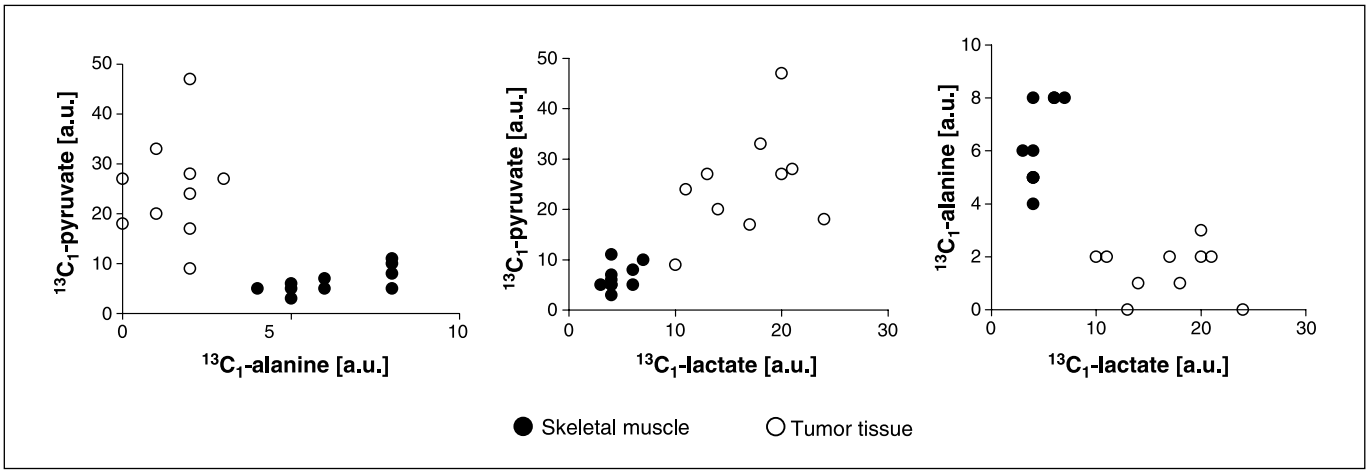

Figure 6. Distribution of the amplitudes for lactate, alanine, and pyruvate for the skeletal muscle and the tumor tissue (n = 10). A clear discrimination between the two tissue types can be seen in all three plots.

Discussion

A direct comparison with existing literature is hampered by the fact that the DNP-MR technique is based on different premises than conventional methods of MR and biochemistry. The DNP-MR technique is dependent on using markers with MR labeling in position with long T_1 (e.g., $^{13}C_1$-pyruvate), whereas conventional ^{13}C-labeling studies prefer short T_1 (e.g., $^{13}C_3$-pyruvate) to be able to collect as many MR pulse averages per time unit as possible. The time scale of the DNP-MR method is different from any study done previously.

It is, therefore, important to use a model with relatively homogenous tissue within the tumor to minimize variability and get data representative of the tissue type. We have implanted P22, a highly malignant rat sarcoma, where central necrosis can be expected to be absent or minor (17–20). The absence of necrotic areas and a homogeneous perfusion profile is important for the interpretation of the data because one has to insure that the injected pyruvate enters the whole tumor area, and that viable cells are available to use the pyruvate into their metabolic pathway. The absence of necrotic areas was confirmed postmortem by histology, whereas the homogeneous perfusion profile was confirmed by performing Gd contrast medium enhanced imaging. Gadodiamide is a 574 Da water-soluble molecule, and the proton images confirmed a homogeneous distribution of the substance within the tumor. It is, therefore, likely that pyruvate, which is a smaller water-soluble molecule with a molecular weight of 110 Da, will distribute at least as well within the 1- to 2-minute time window that is available.

Despite the mentioned difficulties to interpret the data from a classic metabolic modeling point of view, the tumor tissue is in this study clearly indicated by the highest NMR $^{13}C_1$-signal from lactate produced within 30 seconds. The present study shows thereby a direct correlation between the morphologically identified location of the tumor and the location shown by the metabolic lactate image. This finding may support the recent reclaim that a shift in energy production from oxidative phosphorylation to glycolysis is a fundamental property of cancer cells and not just a byproduct of the cell's transformation into cancer (21). The images obtained show that metabolic conversion of pyruvate into alanine and lactate was found in all rats. As expected, when glycolysis dominates (5), lactate production was especially pronounced in all the tumors. The alanine production was high in all normal muscular tissue; however, the tumor cells were equally characterized with low levels of this metabolite. If the metabolism of the injected pyruvate was dominated by Krebs cycle metabolism, we would expect to detect a $^{13}CO_2$ or $H^{13}CO_3^-$ signal. We did not find measurable signal at the relevant frequencies with our current detection limit, and most likely, the concentration of these metabolites is too low in resting muscles and tissue without energy demand (22, 23). In the working heart muscle using a similar technique in pigs, we have detected and characterized the tissue metabolism by means of the $H^{13}CO_3^-$ metabolite.[1]

The interpretation of our data is complicated by the fact that no discrimination can be made between lactate produced in the tumor and lactate produced other places (i.e., in the blood) and delivered to the tumor by perfusion. However, although the current spatial resolution clearly does not allow for accurate tissue selection, the ^{13}C MR-spectra containing the vena cave (Fig. 5*A*) show a clearly different pyruvate to lactate ratio compared with the spectra containing mainly skeletal muscle or tumor tissue. This indicates that the high lactate signal cannot be explained by a high blood volume in the tumor area.

The information obtained by the DNP-MR technique may to some degree mimic what is seen with an FDG-PET/CT image. ^{18}FDG-PET has shown to be a powerful modality for tumor detection and oncology staging. An increased need for glucose transport into the cell is the basis for the use of ^{18}FDG in PET studies. The large amounts of pyruvate taken up by the cancer cells indicate that these cells are very energy demanding. In addition, the almost exclusive conversion of the pyruvate into lactate adds the extra information that cancer cells prefer anaerobic glycolysis despite the abundant presence of oxygen. The DNP-MR technique may, thus, be seen as complementary to the FDG-PET technique in that it reports on the cellular pathways important for the substrate taken up by the cell. In addition, the ^{13}C-MRI offers the possibility for time-resolved quantitative perfusion studies (24).

[1] Submitted to Magnetic Resonance in Medicine.

An improvement in the diagnostic use of PET may be obtained using dual time point ^{18}FDG-PET scans (25) where an indirect measure of glucose transport rate into the cells is obtained using 1 hour between the scans. This, however, would extend the total examination time to 2 hours.

PET has also been used to study the accumulation of ^{11}C-pyruvate in human brain tumors (26). The PET examination, however, does not allow any information about metabolism of the injected substance as does the metabolic imaging method described.

The metabolic transformation of pyruvate into lactate was measured 30 to 44 seconds after the injections. Using lower flip angle pulse makes it realistic to measure the metabolic rate and an image of lactate/pyruvate and lactate/alanine at two or more time points after the injection. The pyruvate, alanine, and lactate images have all been created from the spectra within the same voxels and time frames. This makes it possible to create "ratio images" where, for example, pyruvate can be used as an "internal intravoxel standard." Metabolic ratio and metabolic rate images may, therefore, offer a new type of diagnostic functional information, which could improve the detection and quantification of tumors in the clinical settings.

When MRI was introduced to the clinical community, great expectations were raised since it was claimed (27) that cancer cells would have different T_1 and T_2 values from normal cells. Unfortunately, the normal spread of relaxation times was too high and unspecific to allow cancer identification using these variables. A large number of Gd-labeled vector molecules have also been suggested as markers for cancer by ^{1}H MRI (28). All these molecules are designed to fit into receptors on the cell surface. Thus far, the concentration of receptors has been too low to reveal a significant effect on the contrast to noise in the MRI images.

Pyruvate transformation into lactate seems to occur abundantly in cancer cells, and it is, thus, envisaged that injection of hyperpolarized ^{13}C-labeled pyruvate can be used for early visualization and diagnosis of cancer tissue.

Conclusion

The strong NMR signal produced by the hyperpolarization technique makes metabolic imaging possible. Within a time frame of <1 minute, the transformation of injected pyruvate into alanine and lactate can be imaged noninvasively and may be used to map the metabolic differences between normal and cancerous tissue. The technique that is used in this article (DNP hyperpolarization) is a new and promising possibility for MR in cancer research.

Acknowledgments

Received 7/12/2006; accepted 9/7/2006.

The costs of publication of this article were defrayed in part by the payment of page charges. This article must therefore be hereby marked *advertisement* in accordance with 18 U.S.C. Section 1734 solely to indicate this fact.

References

1. Dawson P, Cosgrove DO, Graninger RG, editors. Textbook of contrast media. San Francisco (CA): Isis Medical Media; 1999.
2. Huisman HJ, Engelbrecht MR, Barentz JO. Accurate estimation of pharmacokinetic contrast-enhanced dynamic MRI parameters of the prostate. J Magn Reson Imaging 2001;13:607–14.
3. Padhani AR. MRI for assessing antivascular cancer treatments. Br J Radiol 2003;76 Spec No 1:S60–80.
4. Board M, Humm S, Newsholme EA. Maximum activities of key enzymes of glycolysis, glutaminolysis, pentose phosphate pathway and tricarboxylic acid cycle in normal, neoplastic and suppressed cells. Biochem J 1990;265:503–9.
5. Xu RH, Pelicano H, Zhou Y, et al. Inhibition of glycolysis in cancer cells: a novel strategy to overcome drug resistance associated with mitochondrial respiratory defect and hypoxia. Cancer Res 2005;65:613–21.
6. Dastidar SG, Sharma SK. Activities of glycolytic enzymes in rapidly proliferating and differentiated C6 glioma cells. Exp Cell Biol 1989;57:159–64.
7. Newsholme EA, Board M. Application of metabolic-control logic to fuel utilization and its significance in tumor cells [review]. Adv Enzyme Regul 1991;31:225–46.
8. Ross BD. The biochemistry of living tissues: examination by MRS [review]. NMR Biomed 1992;5:215–9.
9. Negendank W. Studies of human tumors by MRS: a review [review]. NMR Biomed 1992;5:303–24.
10. Howe FA, Barton SJ, Cudlip SA, et al. Metabolic profiles of human brain tumors using quantitative *in vivo* ^{1}H magnetic resonance spectroscopy. Magn Reson Med 2003;49:223–32.
11. Simonetti AW, Melssen WJ, van der Graaf M, Postman GJ, Heerschap A, Buydens LM. A chemometric approach for brain tumor classification using magnetic resonance imaging and spectroscopy. Anal Chem 2003;75:5352–61.
12. Golman K, Ardenkjaer-Larsen JH, Petersson JS, Mansson S, Leunbach I. Molecular imaging with endogenous substances. Proc Natl Acad Sci U S A 2003;100:10435–9.
13. Ardenkjaer-Larsen JH, Fridlund B, Gram A, et al. Increase in signal-to-noise ratio of >10,000 times in liquid-state NMR. Proc Natl Acad Sci U S A 2003;100:10158–63.
14. Koukourakis MI, Giatromanolaki A, Sivridis E, Gatter KC, Harris AL. Tumor and Angiogenesis Research Group. Pyruvate dehydrogenase and pyruvate dehydrogenase kinase expression in non small cell lung cancer and tumor-associated stroma. Neoplasia 2005;7:1–6.
15. Golman K, in't Zandt R, Thaning M. Real-time metabolic imaging. Proc Natl Acad Sci U S A 2006;103:11270–5.
16. Vanhamme L, Sundin T, Hecke PV, Huffel SV. MR spectroscopy quantitation: a review of time-domain methods. NMR Biomed 2001;14:233–46.
17. Tozer GM, Shaffi KM. Modification of tumour blood flow using the hypertensive agent, angiotensin II. Br J Cancer 1993;67:981–8.
18. Dark GG, Hill SA, Prise VE, Tozer GM, Pettit GR, Chaplin DJ. Combretastatin A-4, an agent that displays potent and selective toxicity toward tumor vasculature. Cancer Res 1997;57:1829–34.
19. Maxwell RJ, Wilson J, Prise VE, et al. "Evaluation of the anti-vascular effects of combretastatin in rodent tumours by dynamic contrast enhanced MRI." NMR Biomed 2002;15:89–98.
20. Prise VE, Honess DJ, Stratford MR, Wilson J, Tozer GM. The vascular response of tumor and normal tissues in the rat to the vascular targeting agent, combretastatin A-4-phosphate, at clinically relevant doses. Int J Oncol 2002;21:717–26.
21. Garber K. Energy boost: the Warburg effect returns in a new theory of cancer. J Natl Cancer Inst 2004;96:1805–6.
22. Schadewaldt P, Munch U, et al. Estimation of pyruvate decarboxylation in perfused rat skeletal muscle. Biochem Biophys Res Commun 1983;116:456–61.
23. Schadewaldt P, Munch U, Staib W. Evidence for the compartmentation of pyruvate metabolism in perfused rat skeletal muscle. Biochem J 1983;216:761–4.
24. Mansson S, Leupold J, Wieben O, et al. Metabolic imaging with hyperpolarized 13C and multi-echo, single shot RARE. Proceedings 14th Scientific Meeting ISMRM, Seattle, WA, 2006.
25. Kumar R, Loving VA, Chauhan A, Zhuang H, Mitchell S, Alavi A. Potential of dual-time-point imaging to improve breast cancer diagnosis with (18)F-FDG PET. J Nucl Med 2005;46:1819–24.
26. Tsukiyama T, Hara T, Iio M, Kido G, Tsubokawa T. Preferential accumulation of ^{11}C in human brain tumors after intravenous injection of ^{11}C-1-pyruvate. Eur J Nucl Med 1986;12:244–8.
27. Damadian R, Zaner K, Hor D, DiMaio T. Human tumors detected by nuclear magnetic resonance. Proc Natl Acad Sci U S A 1974;71:1471–3.
28. Shiftan L, Israely T, Cohen M, et al. Magnetic resonance imaging visualization of hyaluronidase in ovarian carcinoma. Cancer Res 2005;65:10316–23.